A compact broadband ion beam focusing device based on laser-driven megagauss thermoelectric magnetic fields

AIP | Review of Scientific Instruments

A compact broadband ion beam focusing device based on laser-driven megagauss thermoelectric magnetic fields

B. Albertazzi, E. d'Humières, L. Lancia, V. Dervieux, P. Antici, J. Böcker, J. Bonlie, J. Breil, B. Cauble, S. N. Chen, J. L. Feugeas, M. Nakatsutsumi, P. Nicolaï, L. Romagnani, R. Shepherd, Y. Sentoku, M. Swantusch, V. T. Tikhonchuk, M. Borghesi, O. Willi, H. Pépin, and J. Fuchs

Citation: Review of Scientific Instruments **86**, 043502 (2015); doi: 10.1063/1.4917273
View online: http://dx.doi.org/10.1063/1.4917273
View Table of Contents: http://scitation.aip.org/content/aip/journal/rsi/86/4?ver=pdfcov
Published by the AIP Publishing

A compact broadband ion beam focusing device based on laser-driven megagauss thermoelectric magnetic fields

B. Albertazzi,[1,2,3,a)] E. d'Humières,[4,5] L. Lancia,[6] V. Dervieux,[1] P. Antici,[6] J. Böcker,[7] J. Bonlie,[8] J. Breil,[4] B. Cauble,[8] S. N. Chen,[1,8] J. L. Feugeas,[4] M. Nakatsutsumi,[1] P. Nicolaï,[4] L. Romagnani,[1] R. Shepherd,[8] Y. Sentoku,[5] M. Swantusch,[7] V. T. Tikhonchuk,[4] M. Borghesi,[9] O. Willi,[7] H. Pépin,[2] and J. Fuchs[1,b)]

[1]*LULI, École Polytechnique, CNRS, CEA, UPMC, 91128 Palaiseau, France*
[2]*INRS-EMT, Varennes, Québec J3X 1S2, Canada*
[3]*Graduate School of Engineering, Osaka University, Suita, Osaka 565-087, Japan*
[4]*CELIA, Universite de Bordeaux, Talence 33405, France*
[5]*Department of Physics, University of Nevada, Reno, Nevada 89557, USA*
[6]*Dipartimento SBAI, Universita di Roma "La Sapienza," Via A. Scarpa 16, 00161 Roma, Italy*
[7]*Institut für Laser- und Plasmaphysik, Heinrich-Heine-Universität, Düsseldorf D-40225, Germany*
[8]*Lawrence Livermore National Laboratory, Livermore, California 94551, USA*
[9]*School of Physics and Astronomy, The Queen's University, Belfast BT7 INN, United Kingdom*

(Received 30 July 2014; accepted 30 March 2015; published online 13 April 2015)

Ultra-intense lasers can nowadays routinely accelerate kiloampere ion beams. These unique sources of particle beams could impact many societal (e.g., proton-therapy or fuel recycling) and fundamental (e.g., neutron probing) domains. However, this requires overcoming the beam angular divergence at the source. This has been attempted, either with large-scale conventional setups or with compact plasma techniques that however have the restriction of short (<1 mm) focusing distances or a chromatic behavior. Here, we show that exploiting laser-triggered, long-lasting (>50 ps), thermoelectric multi-megagauss surface magnetic (B)-fields, compact capturing, and focusing of a diverging laser-driven multi-MeV ion beam can be achieved over a wide range of ion energies in the limit of a 5° acceptance angle. © *2015 AIP Publishing LLC.* [http://dx.doi.org/10.1063/1.4917273]

I. INTRODUCTION

The possibility of accelerating to high energies (i.e., tens of MeV) ion beams using intense, short-pulse lasers[1,2] has attracted significant attention over the last decade. Indeed, the well-known TNSA (Target Normal Sheath Acceleration) mechanism[3] produces beams with exceptional properties, namely, short (~ps) duration, very high particle number ($\sim 10^{12}$-10^{13}), and extreme laminarity. However, these laser-driven beams also suffer from significant drawbacks at the source, namely, 100% energy spread and a large angular divergence,[4–7] which limit prospects for applications. We should note that new acceleration mechanisms that have been recently proposed can create protons beam having higher energies and lower divergence[8,9] than TNSA. The possibility to focus laser-driven ion (or positron[10]) beams would unlock a wide range of applications ranging from production of radio-isotopes,[11] understanding the mechanisms of extreme energy particle production in Gamma Ray Bursts (GRBs),[12,13] and tests of materials subject to intense particle irradiation such as projected to take place in ITER.[14] It would also improve prospects for proton therapy[15] and for fast ignition of high gain inertial confinement fusion targets.[16]

Several approaches have been studied in order to solve the issue of beam divergence. Long-distance focusing needed for many applications can be achieved with conventional accelerator focusing optics;[17–19] however, this approach involves rather large pieces of equipment. Conversely, plasma-based techniques offer very compact particle focusing setups. For example, use of curved targets has been shown to be effective,[20–23] although limited to short focal distances (<1 mm). Plasma-based focusing lenses have been explored as well where a cylinder is irradiated side-on, thus inducing a transient electric (E)-field in the interior that can focus a proton beam.[24] This has been shown to be successful in capturing and focusing an entire laser-produced ion beam over long distances. However, the target assembly geometry is not straightforward, and more importantly, the focusing of the proton beam varies strongly over its large spectrum due to the short lifetime of the E-fields, typically few ps, i.e., much shorter than the transit time of the protons through the lens. Here, we explore the possibility of using plasma-based strong, long-lived (i.e., thermoelectric) magnetic fields (>50 ps) in order to achieve compact achromatic focusing of a laser-generated proton beam. Its principle and working regime are detailed below.

II. PRINCIPLE OF ION FOCUSING BASED ON ENHANCED THERMOELECTRIC MAGNETIC FIELDS

Magnetic (B) fields spontaneously generated following the irradiation of a solid target by a high power laser are *a priori* very interesting candidates for ion focusing optics. Depending on the characteristics of the laser used, these fields can be produced in varied ways and can have very different properties. One category is *thermoelectric fields*. These fields,

a)bruno.albertazzi@polytechnique.edu
b)Julien.fuchs@polytechnique.fr

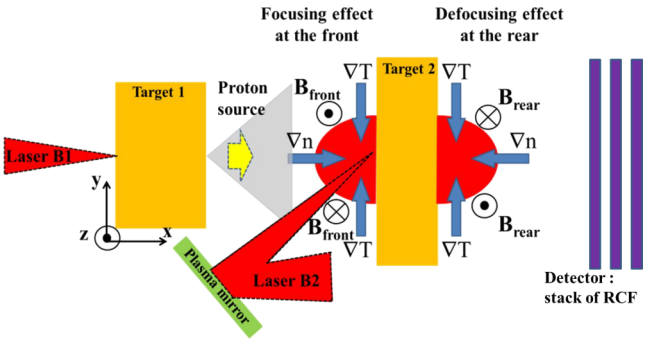

FIG. 1. Sketch of the magnetic proton focusing device proposed here, showing the topology of the thermoelectric B-fields generated on target 2 and their effect on a beam of protons accelerated from target 1.

which appear on the front and rear surfaces of the target, are related to the hydrodynamic expansion of the heated plasma into vacuum (following the laser energy deposition) and are powered by the crossed density and temperature gradients (see Fig. 1).[25,26] They typically appear following high energy nanosecond laser beam irradiation of solid targets and are taken place over the typical time scale of plasma expansion, i.e., nanoseconds.[27–30] As illustrated schematically in Fig. 1, the toroidal geometry and orientation of these fields induce a focusing effect on the front and a defocusing effect at the rear for ions impinging normally to the irradiated target. Due to their hydrodynamic nature, these fields are effective over long time scales (i.e., 100 s of ps), which is long enough to accommodate a large spectrum of energetic ions transiting through the fields. A second category of fields is induced by *hot electron currents* following the irradiation of the target by an intense, short-pulse laser.[31,32] These fields have the same topology as the thermoelectric fields (see Fig. 1) and are of higher amplitude (tens of megagauss (MG)), but are shorter (i.e., ps)—lasting due to the fast damping of the hot electrons within the dense target. Since our goal is to design a B-field structure able to focus the largest band possible of protons transiting through it, we will aim here to exploit the longest-lasting B-fields, i.e., the thermoelectric ones rather than those driven by hot-electrons. Furthermore, there are two design constraints that need to be satisfied: (1) in order to use them to focus efficiently a divergent energetic ion beam, these B-fields need to be very strong (≥MG) and (2) the B-fields at the target front, having a focusing effect, need to predominate over B-fields at the target rear, having a defocusing effect. Since the thermoelectric fields produced by high energy nanosecond laser beams are limited to 1-2 MG,[27–29] which would limit the force acting on transiting ions, here we use sub-picosecond, high intensity, *high contrast* laser beams to produce the thermoelectric B-fields instead. We demonstrate below that this leads indeed to stronger density and temperature gradients (due to the very localized energy deposition in time and space) on the target surface, and hence larger amplitude B-fields (8-10 MG). Although hot electrons induced B-field are produced at the same time, these are quite quickly (10-20 ps) damped, as will be discussed later, and hence, they have little effect on the overall operation of the focusing device. With such larger B-fields, we experimentally show that it is then possible to focus, over a broad spectrum, MeV laser-accelerated protons transiting through the B-field region. Although this focusing device is limited in its angular acceptance (to 5°, as will be detailed below) and thus cannot focus the whole MeV range ion beam that is produced by TNSA mechanisms with 10°-20° (half-angle) divergence,[4–7] it could potentially focus the whole ion beams produced by other acceleration mechanisms, such as RPA (Radiation Pressure Acceleration), which have a lower divergence angle (~4°-5°).[8,9,33]

III. EXPERIMENTAL SETUP

The experiment aimed at demonstrating the effectiveness of using short-pulse lasers to produce an achromatic ion focusing device was performed at the Jupiter Laser Facility's Titan laser at Lawrence Livermore National Laboratory. As shown in Fig. 1, it uses two CPA (Chirped Pulse Amplification) high-energy laser beams, B1 and B2. B1 was used to generate, from target 1 (Au 50 μm thick), the TNSA proton beam to be focused protons with a useful energy range of 3 MeV–10 MeV. B2 was used to generate the B-fields on target 2 (of varied material). Each beam had an energy of approximately 55 J ± 10%, a pulse duration of ~700 fs FWHM, and was focused with a f/3 parabola, resulting in an on-target intensity of $\sim 2 \times 10^{19}$ W/cm^2. B2 was reflected off a plasma mirror (PM), with 70% efficiency, before focus in order to improve its temporal contrast.[34] We had tested that such contrast enhancement was a key factor to produce strong thermoelectric B-fields since otherwise the pre-pulse, i.e., the energy in the laser pulse preceding the main, short-duration, laser pulse, induces a plasma expansion with large-scale gradients, reducing the thermoelectric B-field amplitude. Also, reducing the plasma that can be generated on target 2 ahead of the main pulse reduces the amount of hot electrons that can be produced by B2, hence also reducing the importance of hot-electrons driven B-fields. The proton beam accelerated by B1, and propagated through target 2, was collected by a stack of radiochromic films (RCF). In such stack, protons are deposited in different layers of RCF according to their incident energy.[35]

IV. RESULTS AND DISCUSSION

In order to observe and quantify the ion beam focusability of the proposed magnetic focusing device, we irradiated target 1 with B1 and target 2 with B2 at the same time. This way, the proton beam produced by B1 could then sample a complete sequence of B-fields produced by B2 on target 2. Figure 2(a) shows a typical example of recorded data, with target 2 being here a 3-μm thick Al foil. Target 1 and target 2 are separated by 4 mm and the RCF stack was positioned 39 mm behind target 2. Figs. 2(b)–2(h) correspond to the radial average of the proton dose modulation $\delta n/n$, where $\delta n = n$ (after propagation through the plasma) - n (of the incident proton beam), with n being the proton dose, for each RCF of Fig. 2(a). We first observe at t = 0 (the time B2 irradiates target 2), a depletion of protons in the center ($\delta n/n < 0$) and the protons being accumulated on an outer ring ($\delta n/n > 0$). This corresponds to an overall defocusing effect for the protons

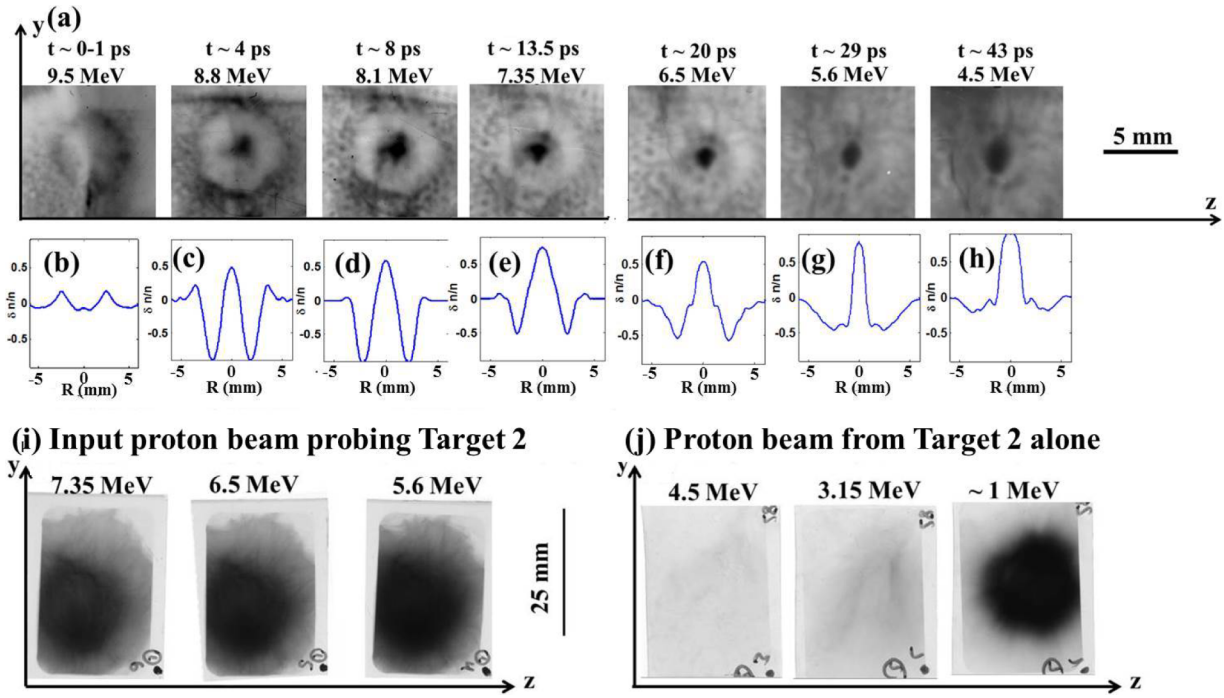

FIG. 2. (a) Typical spatial distribution of protons generated by target 1 (50 μm Au foil) having propagated through target 2 (3 μm Al foil) irradiated by laser beam B2. Darker signal represents an increase of the proton dose. The distance between the stack of RCFs and target 2 is ~3.9 cm. The time t at which protons of a given energy transit through target 2 (t = 0 being the time when B2 irradiates target 2) is indicated above each image, along with the corresponding proton energy. The 5 mm scale indicated by the horizontal bar in the image is given in the plane of the RCF. (b)-(h) present the radial average of the proton dose modulation δn/n associated with the RCFs shown in (a). As a matter of reference, (i) presents, for three proton energies, the proton distribution emitted from target 1, i.e., without having target 2 in place. In this case, target 1 is a 10 μm Au foil. The proton beam emitted by target 1 presents the standard TNSA proton beam angular profile. Similarly, (j) displays the spatial proton distribution generated by target 2 only on the RCFs (there is no target 1 in place in this case). In this case, target 2 is a 3 μm Al foil. The 25 mm scale indicated by the vertical bar shown in between (i) and (j) is given in the plane of the RCF and applied both for (i) and (j).

transiting through target 2 at very early times. However, this defocusing effect disappears after 15 ps. The focusing effect can then be seen to take place. It starts as early as 4 ps and lasts for a duration >40 ps. As shown in Fig. 3, we observe the same global behavior when using several materials for target 2. As a reference, we took shots without target 2 and B2 (see Fig. 2(i)) and verified that the proton beam had the expected divergence.[6,7] We also estimated the proton dose generated by target 2 in taking shots without target 1 and B1 (see Fig. 2(j)). In the case where target 2 was a 3-μm Al thick, for example, the cutoff energy of the proton beam accelerated solely from this target by B2 is ~4.5 MeV (see Fig. 2(j)). At 4.5 MeV, the proton dose is almost negligible (it is more than one order of magnitude less) compared to the proton dose produced from target 1 irradiated by B1 as can be seen in Fig. 2(j). Comparing Figs. 2(i) and 2(j), the dose of the protons accelerated from target 2 by B2 is weaker by more than one order of magnitude compared to the dose of the protons produced from target 1. On the other hand, Fig. 2(i) shows a "normal" profile, i.e., without concentration of the proton dose. Hence, we are sure that the modulations observed on the RCF are really imparted on the probing protons as a result of probing the B-fields developing on target 2 and are not a spurious effect linked to an overlap by the protons produced from target 2.

To quantify the focusing effect resulting from the protons transiting through target 2, we plot in Fig. 3 the experimentally measured proton number density on the RCFs in the central spot, normalized to the standard divergent proton number density (i.e., without B2) on the same RCFs, as a function of the time of transit, as well as of the incident proton energy. Proton number densities are retrieved from measured optical dose of the film through calibration of the film response.[6]

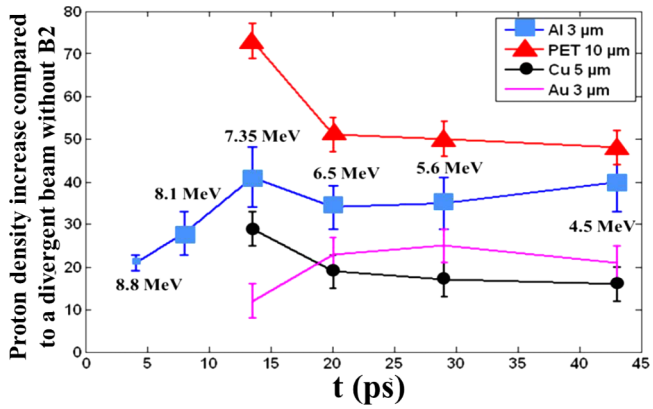

FIG. 3. Increase of proton density in the central spot measured on each RCF compared to the naturally divergent proton density (in vacuum) on the same RCF, showing the focusing effect of the B-field structure triggered on target 2 by laser B2 for different targets of various materials (as indicated). The points in blue squares (target 2 made of 3-μm thick Al foil) correspond to the data of Fig. 2. The overall trend shows that the focusing effect is more pronounced at lower material density. The time t corresponds to the time at which protons of a given energy transit through target 2 (t = 0 being the time when B2 irradiates the target 2).

We clearly observe that past an early phase of competition between defocusing and focusing effects, the focusing effect dominates and becomes steady, leading to a constant dose increase for the various energy protons transiting through target 2. An interesting feature observed in Fig. 3 is that the thickest target (polyethylene terephthalate PET) exhibits a higher increase of density of the probing protons at early times. This could be due to a weaker early defocusing effect related to the rear surface B-field as the electron density at the rear surface of the target is reduced for thicker targets, but since for this shot the probing protons were not energetic enough to measure the B-fields at times as early as for the Al target case, we cannot conclude on this point.

To get a detailed insight into the B-fields acting on the protons, we now derive the values of the effective front and rear magnetic fields. This is done by comparing the experimental protons deflections measured on the RCFs with simulated deflections using a B-field dependent particle tracing code, as detailed in Ref. 28. The particle tracer simulates the trajectories of a homogeneous monoenergetic beam of protons through a 2D B-field map, producing as output, a lineout of the induced modulation of the proton density on the detector plane. The diffusion due to scattering in a solid target is also included. The B-field map is modeled according to the geometry of the B-fields suggested by simulations involving both a 2D particle in cell (PIC) code (PICLS)[36] and a 2D magnetohydrodynamic (MHD) code (CHIC)[37] in order to accommodate the very different time scales at play (the details of the simulations will be reported in a longer paper to follow). The result of this analysis giving the inferred B-fields is shown in Fig. 4. The typical geometry allowing to retrieve the experimental data is (i) a typical length of the B-fields in the x direction (see Fig. 1) of 5 μm, (ii) a radial extend of the order of ~100 μm, and (iii) a typical amplitude of 8-10 MG. We clearly see that the early defocusing is due to the dominant rear surface B-field, the intermediate phase with both focusing and defocusing is due to the presence of both rear and front B fields, and the solely focusing effect is due to the dominant front surface B-field at late times. Thus, one can see that by simply delaying B2 in time compared to B1 by ~15 ps, one can avoid entirely the defocusing stage and see the central part of the proton beam originating from target 1 be focused after passing through target 2.

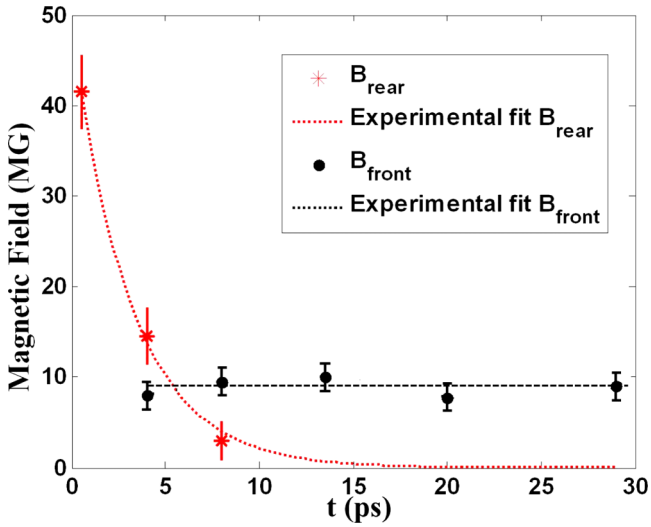

FIG. 4. Front and rear magnetic fields inferred from the Al experimental data (shown in Fig. 1) using a B-field dependent particle tracing code and taken at the center of the magnetic field zone for a given time.

More precisely, we observe in our 2D PIC simulations that the early dominant, and proton defocusing, rear B-field is generated by hot electrons, in line with the previous analysis of Ref. 32 where the B-field is confined at both surfaces of the Al target in a layer of 0.1-1 μm and extends radially over more than 100 μm which corresponds to the length of the simulation box in the y direction (see Fig. 1). This B-field leads to an overall divergence of the proton beam with an annular concentration of protons as observed in the experiments. However, this B-field is dissipated progressively as the hot electrons transfer their energy to the target bulk and cool down. Using a 1D three temperature model to simulate the energy exchange between hot electrons, cold (bulk) electrons, and bulk ions,[38] we find for Al that after ~20 ps, the hot electron driven B-fields disappear, which is consistent with the data of Figs. 2-4. For Au, the cooling time is found to be longer, again in agreement with the data of Fig. 3 where we observe that stable focusing takes place after a longer time compared to Al. It is thus preferable to use low-Z materials to quickly quench the defocusing B-fields. Moreover, high-Z materials also scatter more the transiting protons, hence reducing the effective proton density in the focusing spot, as can be seen in Fig. 3. This points to the preferred use of low-Z materials for the focusing device.

The azimuthal thermoelectric B-fields appear while the hot electrons induced B-fields are still present. At the target front surface, they are driven by the strong temperature and density gradients related to the narrow laser irradiation region (~8 μm) and high laser pulse contrast. At the target rear, they are also driven by the temperature gradients, which are there smoother (as the hot electrons induced heating is spatially spread over a large area, ~100 μm), as has already been measured using a time-and-space resolved technique.[39] The rear-surface B-fields will thus be of lower amplitude than those at the front, in agreement with what is experimentally inferred (see Fig. 4). It should be noted that compared to Ref. 32, we only used one experimental configuration (irradiating target 2 from the front) due to the constraint presented by the use of a plasma mirror. This allowed us to deduce at early times only the rear surface B-fields. The dominant front surface thermoelectric B-field, as studied with the hydrodynamic code CHIC, lasts for a long time (>50 ps) and produces the overall long-lasting focusing observed in Figs. 2 and 3.

Using the B-field inferred from Fig. 4 and the particle tracer, we can simulate the trajectories of the protons in space after passing through target 2. In particular, we can calculate the FWHM of the focused proton spot (the central black dot that can be seen in Fig. 2) along the beam propagation. This diameter is presented in Fig. 5 for two proton energies as a function of the distance (1-10 cm) from target 2. The simulated and measured spot size, at the location of the RCF, agrees. We further observed that the focused spot size remains relatively small even at large distances, especially when comparing it

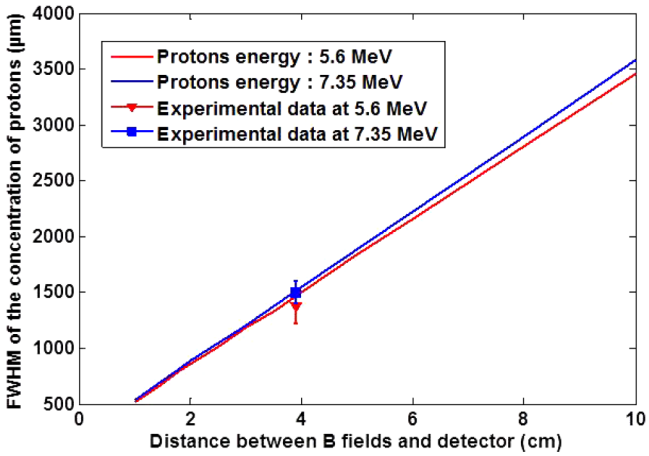

FIG. 5. FWHM of the focused central spot of protons (as seen in Fig. 1) as a function of the distance from target 2 for two different proton energies (7.35 MeV and 5.6 MeV). The experimental data for the two proton energies are overlaid.

to the size the beam would have as a result of its natural divergence: at 10 cm, instead of being 1.7 cm wide (accounting only for the beam within the 5° aperture subtended by the B-fields), the beam, focused by the B-fields, is only 3.5 mm, with a related flux increase of ~25. We also note that the diameter remains quite the same for a large span of proton energies (3 MeV–10 MeV), as could already be seen in Fig. 2.

One drawback, related to the limited strength and extent of the B-field on the target surface, is that only part of the TNSA divergent proton beam can be captured and deflected by the front surface B-field and thus results in the focused spot observed in Fig. 2. This is due to the fact that the change of perpendicular momentum imparted by the B field to the protons is given by $\Delta p_y = -qBL_{B_z}$, where L_{B_z} is the width of the B-field along x (see Fig. 1). For protons to be deflected, one needs a reversal of p_y, which defines the maximum angle at which protons can be incident on the B-field structure and still be deflected or focused. Protons coming at larger angle will just see their divergence reduced but will not be focused. We can then express the change of the transverse velocity component (i.e., in the y direction) of a proton passing through a magnetic field, which is given by

$$v_{\perp final} = v_{\perp initial} - \frac{qB_zL_{B_z}}{m},$$

where $v_{\perp initial}$ (respectively, $v_{\perp final}$) is the initial (respectively, final) transverse velocity of the proton, q is the elementary electric charge, B_z is the magnetic field amplitude, and m is the proton mass. As can be seen in the above equation, the collimation factor $\frac{qB_zL_{B_z}}{m}$ is independent from the proton energy, meaning that in order to collimate a proton beam (this principle can be extended to ion beam), the divergence angle of the beam must be rather small in order to have a strong focusing effect. Experimentally, we can deduce from Fig. 2 the area on target 2 over which protons have been able to be captured and focused. This area subtends an angle of 5° from target 1, hence only this inner cone, containing ~5% of the protons, out of the ~20° divergent beam, can be focused.

Another interesting information obtained from simulations is that if we want the device to work effectively, the intensity of laser beam B2 should stay within the range 10^{19}–10^{20} W/cm^2. At higher intensities, the cooling time of the hot electrons is indeed longer and it would take more time for the hot electrons induced B-fields to disappear. At lower intensities, the final bulk temperature would be too small (10-20 eV) to generate a multi-MG B-field through the thermoelectric effect. A relevant bulk temperature should be of the order of ~80-90 eV,[40] which corresponds to an intensity of $\sim 5 \times 10^{19}$ W cm^{-2}. Moreover, at the front surface, due to the high laser contrast, the temperature gradient should be steeper than the one at the back, leading to a magnetic field in the MG range. As a practical example, with a T_e ~ 80-100 eV, a laser pulse of 700 fs, and an Al target with $Z^* = 9$, we obtain using the formula developed in Ref. 41 $L_n \sim 0.05 - 0.1$ μm and taking a realistic value of $L_T \sim 2$ μm (as inferred from the PICLS simulations) the amplitude of the B-fields at the front surface is of the order of few to tens MG using the following equation:[42]

$$B[T] \approx 1.0004 \left(\frac{\mu m}{L_n}\right)\left(\frac{T_e}{eV}\right)\left(\frac{\mu m}{L_T}\right)\left(\frac{\tau}{ps}\right),$$

where L_n is the density gradient scale length, T_e is the electron temperature, L_T is the temperature gradient scale length, and τ is the laser pulse duration.

V. CONCLUSION

In conclusion, we have shown that ~10 MG, long-lived, surface toroidal magnetic field can be produced by high intensity, high contrast laser irradiating a solid target. These can be used to capture and refocus a large energy range of diverging, laser-produced protons. Effective control of proton focusing can be directly achieved by varying (i) the delay between the laser pulse that produces the protons beams and the laser pulse that is used to generate the self-generated magnetic field, (ii) the material of the target onto which the B-fields are generated, and (iii) the target thickness. Such device offers a compact, simple solution to concentrate protons (or ions) transiting through the B-fields configuration. We have shown that the critical parameters to achieve efficient focusing are (i) a high contrast of the laser triggering the B-fields (which can be achieved by using a frequency-doubled laser rather than using a plasma mirror), (ii) a laser intensity for B2 in the range 10^{19}-10^{20} W cm^{-2}, and (iii) thin target (few micrometer) of low Z material in order to favor the focusing front B-field and minimize proton scattering through the target. Using TNSA-generated beams, the device does not allow the capture of the entire divergent proton beam from the source. However, the device could be an excellent match to ion beams produced by emerging acceleration mechanisms[8] that have intrinsically a very low divergence, as suggested by recent measurements,[9] and could attain very high energies.

ACKNOWLEDGMENTS

We acknowledge the expert support of the LLNL teams. This work was supported by grant E1127 from Région Ile-de-France, by the National Science Foundation, Grant No. 1064468, ELAM and ULIMAC grants from the Triangle

de la Physique RTRA network, and by NSERC Discovery Grant No. 26558-2007 RGPIN from Canada. O.W. would like to acknowledge DFG Programme GRK 1203. This work was partly done within the LABEX Plas@Par project and received financial state aid managed by the Agence Nationale de la Recherche, as part of the program "Investissements d'avenir" under the reference ANR-11-IDEX-0004-02. The research leading to these results has also received funding from LASERLAB-EUROPE (Grant Agreement No. 284464, EC's Seventh Framework Programme), Grant No. 001528, and from EPSRC, Grant No. EP/K022415/1. This work is also partly supported by the EURATOM within the "Keep-in-Touch" activities and the Aquitaine Regional Council.

[1]H. Daido, M. Nishiuchi, and A. S. Pirozhkov, Rep. Prog. Phys. **75**, 056401 (2012); A. Macchi, M. Borghesi, and M. Passoni, Rev. Mod. Phys. **85**, 751-793 (2013).
[2]J. Fuchs, P. Audebert, M. Borghesi, H. Pépin, and O. Willi, C. R. Phys. **10**, 176 (2009).
[3]S. C. Wilks, W. L. Kruer, M. Tabak, and A. B. Langdon, Phys. Rev. Lett. **69**, 1383 (1992).
[4]E. Brambrink, J. Schreiber, T. Schlegel, P. Audebert, J. Cobble, J. Fuchs, M. Hegelich, and M. Roth, Phys. Rev. Lett. **96**, 154801 (2006).
[5]F. Nurnberg, M. Schollmeier, E. Brambrik, A. Blazevic, D. C. Carroll, K. Flippo, D. C. Gauthier, M. Geissel, K. Harres, B. M. Hegelich, O. Lundh, K. Markey, P. Mckenna, D. Neely, J. Schreiber, and M. Roth, Rev. Sci. Instrum. **80**, 033301 (2009).
[6]A. Mancic, J. Robiche, P. Antici, P. Audebert, C. Blancard, P. Combis, F. Dorchies, G. Faussurier, S. Fourmaux, M. Harmand, R. Kodama, L. Lancia, S. Mazevet, M. Nakatsutsumi, O. Peyrusse, P. Renaudin, R. Shepherd, and J. Fuchs, High Energy Density Phys. **6**, 21 (2010).
[7]P. R. Bolton, M. Borghesi, C. Brenner, D. C. Caroll, C. De, A. Martinis, V. Flacco, J. Floquet, P. Fuchs, D. Gallegos, J. S. Giove, S. Green, B. Green, D. Jones, P. Kirby, D. Mckenna, F. Neely, R. Nuesslin, S. Prasad, M. Reinhardt, U. Roth, G. G. Schramm, A. Scott, M. Ter-Avertisyan, G. Tolley, J. J. Turchetti, and Wilkens, Phys. Med. **30**, 255-270 (2014).
[8]A. P. L. Robinson, M. Zepf, S. Kar, R. G. Evans, and C. Bellei, New J. Phys. **10**, 013021 (2008).
[9]J. H. Bin, W. J. Ma, K. Allinger, H. Y. Wang, D. Kiefer, S. Reinhardt, P. Hilz, K. Khrennikov, S. Karsch, X. Q. Yan, F. Krausz, T. Tajima, D. Habs, and J. Schreiber, Phys. Plasmas **20**, 073113 (2013).
[10]H. Chen, S. C. Wilks, J. D. Bonlie, E. P. Liang, J. Myatt, D. F. Price, D. D. Meyerhofer, and P. Beiersdorfer, Phys. Rev. Lett. **102**, 105001 (2009).
[11]M. I. K. Santala, Z. Najmudin, E. L. Clark, M. Tatarakis, K. Krushelnick, A. E. Dangor, V. Malka, J. Faure, R. Allott, and R. J. Clarke, Appl. Phys. Lett. **78**, 19-21 (2001); S. Fritzler, V. Malka, G. Grillon, J. P. Rousseau, F. Burgy, E. Lefebvre, E. d'Humières, P. Mc Kenna, and K. W. D. Ledingham, Appl. Phys. Lett. **83**, 3039 (2003).
[12]S. P. Davis, V. Tikhonchuk, E. d'humières, and S. Weber, J. Phys.: Conf. Ser. **244**, 042006 (2010); S. P. Davis, R. Capdessus, E. d'Humières, S. Jequier, I. Andriyash, and V. Tikhonchuk, High Energy Density Phys. **9**, 231 (2013).
[13]A. Spitkovsky, Astrophy J. **673**, L39 (2008).
[14]T. J. Renk, C. L. Olson, T. J. Tanaka, M. A. Ulrickson, G. A. Rochau, R. R. Peterson, I. E. Golovkin, M. O. Thompson, T. R. Knowles, A. R. Raffray, and M. S. Tillack, Fusion Eng. Des. **65**, 399-406 (2003).
[15]S. V. Bulanov, T. Zh, V. S. Esirkepov, A. V. Khoroshkov, F. Kuznestov, and Pegoraro, Phys. Lett. A **299**, 240 (2002); V. Malka, S. Fritzler, E. Lefebvre, E. d'Humières, R. Ferrand, G. Grillon, C. Albaret, S. Meyroneinc, J.-P. Chambaret, A. Antonetti, and D. Hulin, Med. Phys. **31**, 1587 (2004).
[16]M. Roth, T. E. Cowan, M. H. Key, S. P. Hatchett, C. Brown, W. Fountain, J. Johnson, D. M. Pennington, R. A. Snavely, S. C. Wilks, K. Yasuike, H. Ruhl, F. Pegoraro, S. V. Bulanov, E. M. Campbell, M. D. Perry, and H. Powell, Phys. Rev. Lett. **86**, 436 (2001).
[17]M. Schollmeier, S. Becker, M. Geissel, K. A. Flippo, A. Blazevic, S. A. Gaillard, D. C. Gautier, F. Gruner, K. Harres, M. Kimmel, F. Nurnberg, P. Rambo, U. Schramm, J. Schreiber, J. Schutrumpf, J. Schwarz, N. A. Tahir, B. Atherton, D. Habs, M. Hegelich, and M. Roth, Phys. Rev. Lett. **101**, 055004 (2008).
[18]J. Teng, Y. Q. Gu, B. Zhu, W. Hong, Z. Q. Zhao, W. M. Zhou, and L. F. Cao, Nucl. Instrum. Methods Phys. Res., Sect. A **729**, 399–403 (2013).
[19]S. Busold, D. Schumacher, O. Deppert, C. Brabetz, F. Kroll, A. Blažević, V. Bagnoud, and M. Roth, Phys. Rev. Spec. Top.–Accel. Beams **17**, 031302 (2014).
[20]P. K. Patel, A. J. Mackinnon, M. H. Key, T. E. Cowan, M. E. Foord, M. Allen, D. F. Price, H. Ruhl, P. T. Springer, and R. Stephens, Phys. Rev. Lett. **91**, 125004 (2003).
[21]T. Bartal, M. E. Foord, C. Bellei, M. H. Key, K. A. Flippo, S. A. Gaillard, D. T. Offermann, P. K. Patel, L. C. Jarott, D. P. Higginson, M. Roth, A. Otten, D. Kraus, R. B. Stephens, H. S. Mclean, E. M. Giraldez, M. S. Wei, D. C. Gautier, and F. N. Beg, Nat. Phys. **8**, 139 (2012).
[22]S. Kar, K. Markley, M. Borghesi, D. C. Caroll, P. Mckenna, D. Neely, M. N. Quinn, and M. Zepf, Phys. Rev. Lett. **106**, 225003 (2011).
[23]S. N. Chen, E. d'Humières, E. Lefebvre, L. Romagnani, T. Toncian, P. Antici, P. Audebert, E. Brambrink, C. A. Cecchetti, T. Kudyakov, A. Pipahl, Y. Sentoku, M. Borghesi, O. Willi, and J. Fuchs, Phys. Rev. Lett. **108**, 055001 (2012).
[24]T. Toncian, M. Borghesi, J. Fuchs, E. d'Humières, P. Antici, P. Audebert, E. Brambrink, C. A. Cecchetti, A. Pipahl, L. Romagnani, and O. Willi, Science **312**, 410-413 (2006).
[25]S. I. Braginskii, *Reviews of Plasma Physics*, edited by M. A. Leontovich (Consultants Bureau, New York, 1965), Vol. 1.
[26]J. A. Stamper, Laser Part. Beams **9**, 841-862 (1991).
[27]L. Lancia, C. Fourment, J. Fuchs, J.-L. Feugeas, Ph. Nicolai, S. Bastiani-Ceccotti, M. Gauthier, S. Hulin, M. Nakatsutsumi, M. Rabec-Le-Gloahec, J. J. Santos, and G. Schurtz, Laser Part. Beams **31**, 653–661 (2013).
[28]C. K. Li, F. H. Séguin, J. A. Frenje, J. R. Rygg, R. D. Petrasso, R. P. J. Town, P. A. Amendt, S. P. Hatchett, O. L. Landen, A. J. Mackinnon, P. K. Patel, M. Tabak, J. P. Knauer, T. C. Sangster, and V. A. Smalyuk, Phys. Rev. Lett. **99**, 015001 (2007).
[29]C. A. Cecchetti, M. Borghesi, J. Fuchs, P. A. Wilson, P. Antici, P. Audebert, L. Romagnani, O. Willi, T. Toncian, R. Young, C. A. Pipahl, A. M. M. Schiavi, and G. Schurtz, Phys. Plasmas **16**, 043102 (2009).
[30]M. Borghesi, A. J. Mackinnon, A. R. Bell, R. Gaillard, and O. Willi, Phys. Rev. Lett. **81**, 112 (1998).
[31]P. Kolodner and E. Yablonovitch, Phys. Rev. Lett. **37**, 1754 (1976).
[32]G. Sarri, A. Macchi, C. A. Cecchetti, S. Kar, T. V. Liseykina, X. H. Yang, M. E. Dieckmann, J. Fuchs, M. Galimberti, L. A. Gizzi, R. Jung, I. Kourakis, J. Osterholz, F. Pegoraro, A. P. L. Robinson, L. Romagnani, O. Willi, and M. Borghesi, Phys. Rev. Lett. **109**, 205002 (2012).
[33]B. Aurand *et al.*, J. New Phys. **15**(3), 033031 (2013); D. Jung *et al.*, New J. Phys. **15**(2), 023007 (2013); D. Jung *et al.*, Phys. Plasmas **20**, 083103 (2013); S. Kar *et al.*, Phys. Rev. Lett. **109**, 185006 (2012).
[34]G. Doumy, F. Quéré, O. Gobert, M. Perdrix, Ph. Martin, P. Audebert, J. C. Gauthier, J.-P. Geindre, and T. Wittmann, Phys. Rev. E **69**, 026402 (2004).
[35]P. R. Bolton, M. Borghesi, C. Brenner, D. C. Carroll, C. De, A. Martinis, V. Flacco, J. Floquet, P. Fuchs, D. Gallegos, J. S. Giove, S. Green, B. Green, D. Jones, P. Kirby, D. Mckenna, F. Neely, R. Nuesslin, S. Prasad, M. Reinhardt, U. Roth, G. G. Schramm, A. Scott, M. Ter-Avetisyan, G. Tolley, J. J. Turchetti, and Wilkens, Phys. Med. **30**, 255-270 (2014).
[36]Y. Sentoku and A. J. Kemp, J. Comput. Phys. **227**, 6846 (2008).
[37]P.-H. Maire, R. Abgrall, J. Breil, and J. Ovadia, SIAM J. Sci. Comput. **29**, 1781 (2007).
[38]P. Antici, L. Gremillet, T. Grismayer, P. Mora, P. Audebert, M. Borghesi, C. A. Cecchetti, A. Mancic, and J. Fuchs, Phys. Plasmas **20**, 123116 (2013).
[39]P. Antici, J. Fuchs, M. Borghesi, L. Gremillet, T. Grismayer, Y. Sentoku, E. d'humieres, C. A. Cecchetti, A. Mancic, A. C. Pipahl, T. Toncian, O. Willi, P. Mora, and P. Audebert, Phys. Rev. Lett. **101**, 105004 (2008).
[40]B. Albertazzi *et al.*, "Dynamics and structure of self-generated magnetic fields on solids following high contrast, high intensity laser irradiation," Phys. Plasmas (submitted).
[41]W. L. Kruer, Plasma Phys. Controlled Fusion **9**, 63 (1985).
[42]M. G. Haines, Phys. Rev. Lett. **78**, 254 (1997).